JOURNAL OF GEOPHYSICAL RESEARCH, VOL. 114, B12401, doi:10.1029/2008JB006037, 2009

Geologic evidence for multiple slip weakening mechanisms during seismic slip in crystalline rock

J. D. Kirkpatrick[1] and Z. K. Shipton[1]

Received 26 August 2008; revised 12 August 2009; accepted 19 August 2009; published 5 December 2009.

[1] We examine exhumed seismogenic faults to investigate the mechanisms that may have achieved dynamic fault weakening during ancient ruptures. Field and microscope observations imply more than one weakening mechanism must have been active during slip events on the faults. Pseudotachylytes that are continuous over the scale of field exposures are indicative of melt lubrication. A fault breccia crosscutting earlier formed cataclasites was mobilized during faulting and possibly represents a pressurized fault rock that resulted from thermal pressurization or elastohydrodynamic lubrication. In some faults, pseudotachylytes are developed in patches several meters long. Cataclasites in which there is no evidence for melting are present immediately along strike from the pseudotachylyte patches. By considering the energy required for melting, we show that the pseudotachylytes must have formed during ruptures larger than the patches, implying that the cataclasites also accommodated seismic slip. The distribution of fault rock types shows that the frictional response to slip during a single event was spatially variable. Reworked pseudotachylytes also indicate that coseismic processes change over time at a point on a fault. These observations emphasize that macroscopic dynamic fault weakening is a function of multiple coeval processes at microscales to mesoscales. Detailed observations of the discontinuous pseudotachylytes show that slip zone thickness is the critical parameter that controls active coseismic processes. The frictional response of a fault to slip is therefore dependent on the internal structure of faults; given the along-strike heterogeneity of most mapped fault zones, the coexistence of multiple slip weakening mechanisms in a single earthquake will be common.

Citation: Kirkpatrick, J. D., and Z. K. Shipton (2009), Geologic evidence for multiple slip weakening mechanisms during seismic slip in crystalline rock, *J. Geophys. Res.*, *114*, B12401, doi:10.1029/2008JB006037.

1. Introduction

[2] Earthquake rupture propagation is controlled by the rheological response of the slip zone to coseismic slip. Fault instability requires the strength of a fault to decrease more rapidly than the release of tectonic stresses, implying that faults weaken as slip progresses (see reviews by *Rice and Cocco* [2007] and *Cocco and Tinti* [2008]). The classic slip weakening model describes the change in strength of a fault from an initial static value, τ_o, to a steady state dynamic value, τ_f (often associated with the frictional sliding resistance [*Cocco and Tinti*, 2008]), following rupture initiation when the yield stress, τ_y, of a fault is exceeded [e.g., *Ida*, 1972; *Andrews*, 1976]. The rate at which the reduction in strength occurs is characterized by the slip weakening distance D_c, which is the amount of slip required to achieve τ_f. The manner in which the frictional strength of a fault changes is inherently related to stress drop, slip magnitude and slip velocity through the slip weakening model, and is of fundamental importance to energy partitioning during an earthquake [*Kanamori and Rivera*, 2006; *Cocco and Tinti*, 2008].

[3] Coseismic fault slip is observed to be spatially and temporally variable at a variety of scales [*Mai and Beroza*, 2002; *Aochi and Ide*, 2009, and references therein]. Estimates of D_c for earthquakes from seismological data generally yield values of tens of centimeters to a meter (e.g., ~1 m [*Bouchon et al.*, 1998]; ~0.4 m [*Ide*, 2002]) and in some cases are shown to vary spatially for a single event (0.5 to 1 m [*Ide and Takeo*, 1997]; 0.4 to 0.9 m [*Mikumo et al.*, 2003]). Finite source inversions also show that dislocation rise times, slip distributions and static stress drops are heterogeneous for a single rupture event [e.g., *Beroza and Spudich*, 1988; *Cohee and Beroza*, 1994; *Sekiguchi et al.*, 2000]. These spatial variations are thought to occur because the prerupture shear stress field [*Das and Aki*, 1977] and/or the fault friction [e.g., *Kanamori and Stewart*, 1978] are spatially heterogeneous. However, dynamic rupture simulations that constrain D_c and shear stress by matching recorded strong motion data are not able to distinguish spatial variations in the frictional response to slip. Such simulations provide nonunique solutions that are unable to differentiate between scenarios of homogeneous shear stress

[1]Department of Geographical and Earth Sciences, University of Glasgow, Glasgow, UK.

0148-0227/09/2008JB006037$09.00

and heterogeneous D_c and *vice versa* [e.g., *Guatteri and Spudich*, 2000; *Peyrat et al.*, 2004].

[4] The coseismic processes that have been proposed to achieve a dynamic reduction in the strength of a fault (slip weakening mechanisms) include thermal pressurization [*Sibson*, 1973; *Lachenbruch*, 1980], flash heating [*Rice*, 2006; *Rice and Cocco*, 2007], elastohydrodynamic lubrication [*Brodsky and Kanamori*, 2001], melt lubrication [*Jeffreys*, 1942; *McKenzie and Brune*, 1972; *Di Toro et al.*, 2006], silica gel formation [*Di Toro et al.*, 2004], acoustic fluidization [*Melosh*, 1996] and normal interface vibration [*Brune et al.*, 1993]. In natural faults, the slip weakening mechanisms that are active in the slip zone control the frictional response to slip and will be influenced by fault zone properties such as grain size distribution and permeability of fault rocks in and around the slip zone, the presence or absence of fluids, and the melting temperature of the material in the slip zone [e.g., *Rice*, 2006]. Faults that have a long and complex history are often structurally heterogeneous. Faults are observed to comprise macroscale discontinuities such as bends and step overs [*King and Nabelek*, 1985; *Wesnousky*, 2006], juxtapose different rock types along strike [e.g., *Dor et al.*, 2006], frequently display changeable macroscale architecture along strike [e.g., *Faulkner et al.*, 2003], and also contain a variety of deformation products [e.g., *Evans*, 1990]. The dependence of slip weakening mechanisms on the physical properties of fault rock assemblages suggests that fault complexity will influence rupture propagation. Constraining the interaction between fault structure and coseismic processes could therefore provide insight into the causes of spatial variations in seismic source parameters.

[5] Fault zones exhumed from the depths at which earthquakes nucleate provide an opportunity to study the seismic source in detail. Field studies of exhumed faults are necessarily restricted by the degree of exposure of any particular structure, limiting the extent to which direct correlations can be made between field and seismic data. For example, the observations presented in this study document the structure of seismogenic faults at the meter to tens of meters scale, whereas the inversion of seismic data typically has a minimum spatial resolution of hundreds of meters. However, *Aagaard and Heaton* [2008] point out that frictional stress changes occur over a few milliseconds, suggesting that corresponding slip weakening distances, or breakdown zone widths, might be of the order of millimeters. The relatively short length scales exposed in the field are therefore of relevance to the rupture process. Ancient fault zones can be used to investigate rupture processes if the faults can be shown unequivocally to have experienced ancient earthquakes [e.g., *Di Toro et al.*, 2005a]. To date, the only fault rock type that is a certain indicator of past earthquake ruptures along ancient faults are pseudotachylytes, the cooled remnants of melts formed by frictional heating during slip at seismic slip rates [*Cowan*, 1999].

[6] We present observations of pseudotachylyte-bearing faults exhumed from seismogenic depths in the Sierra Nevada, California, with the aim of (1) attempting to identify slip weakening mechanisms and (2) investigating spatial and temporal variations in the frictional response of the slip zone to coseismic slip. The faults vary in composition along strike and contain both cataclasites and pseudotachylytes. By considering the energy required for melting, we show that pseudotachylytes developed in patches meters long can only have formed during earthquakes that ruptured a length of the fault greater than the length of the pseudotachylytes. At least some of the adjacent cataclastic rocks must also have therefore formed during the same events. Given the observed variability in fault rock type and composition, the faults contain evidence for multiple slip weakening mechanisms as well as a spatially variable frictional response to slip during a single rupture. Our combined outcrop and microscope scale observations indicate that the fault structure controls the active coseismic processes, suggesting that fault heterogeneity plays a critical role in controlling dynamic fault weakening.

2. Predicted Microstructural Evidence for Slip-Weakening Mechanisms

[7] In this section we review previously described slip weakening mechanisms with the intention of determining what deformation products each mechanism might leave in a fault zone that could be used for the purpose of identification. We emphasize here that although the observation of pseudotachylyte in a fault is the strongest possible evidence that the fault accommodated at least part of its total slip through coseismic rupture [*Cowan*, 1999], the absence of pseudotachylytes doesn't automatically mean that the fault developed entirely through aseismic processes. In fact, many mature fault zones do not appear to contain pseudotachylyte, suggesting that alternative slip weakening mechanisms must be involved during earthquakes on these faults. However, at present there are no generic criteria that distinguish cataclasites generated during fast seismic slip from those generated by aseismic slip (i.e., subseismic rupture duration or particle velocities, as defined by *Cowan* [1999]) or by quasi-static processes during an interseismic period. Identifying slip weakening mechanisms from observations of cataclasites is therefore problematic in the absence of associated pseudotachylytes.

[8] Melt lubrication is an effective slip weakening mechanism if a continuous layer of melt forms during slip [*McKenzie and Brune*, 1972; *Fialko and Khazan*, 2005; *Hirose and Shimamoto*, 2005; *Di Toro et al.*, 2006], and is the best described slip weakening mechanism in natural faults. The structural organization of pseudotachylyte veins within faults shows that pseudotachylytes are generated by frictional heating along slip zones, and therefore record the occurrence of melt lubrication during past seismic events [*Sibson*, 1975]. To demonstrate a melt origin for these rocks compositional and textural characteristics of rapidly quenched melt must be observed, requiring optical and scanning electron microscope analyses, though fresh glass is rarely reported [*Maddock*, 1983; *Magloughlin and Spray*, 1992]. In the Sierra Nevada, pseudotachylytes have recently been identified in a number of faults [*Griffith et al.*, 2008; *Kirkpatrick et al.*, 2008, 2009]. Studies of pseudotachylyte bearing faults have used field observations to calculate coseismic shear resistance [*Sibson*, 1975; *Killick and Roering*, 1998; *Barker*, 2005; *Di Toro et al.*, 2006], slip weakening distance [*Di Toro et al.*, 2005b], energy partitioning [*Pittarello et al.*, 2008] and static stress drops [*Barker*, 2005].

[9] Flash heating involves heat generation at microscale to nanoscale asperity contacts across a sliding surface [e.g., *Rice*, 2006; *Beeler et al.*, 2008]. The physical products of flash heating should be deformed asperity contacts, non-melting grain breakdown products, and small (microscale to nanoscale) pockets of quenched melt at asperity boundaries [*Beeler et al.*, 2008]. Rapid slip experiments to determine the frictional properties of quartz-rich rocks have shown a velocity-dependent weakening that is thought to be brought about by the formation of a thin layer of silica gel at asperity contacts [*Di Toro et al.*, 2004]. Silica gel, which is composed of an amorphous silica-water mix, might therefore form thin films of amorphous material coating a fault surface. The potential signatures of both flash heating and silica gel formation are exceptionally fine scale, and the likelihood of small amounts of solidified melt or gel remaining without being subsequently deformed or chemically altered in a fault zone seems low.

[10] Thermal pressurization [e.g., *Sibson*, 1973; *Lachenbruch*, 1980] requires fluid-filled pore spaces in the slip zone. After the onset of slip, frictional heating causes thermal expansion of the fluid phase, and if the fluid cannot escape this reduces the effective normal stress and therefore shear strength across the slip zone. This mechanism is considered to work in combination with other thermally driven processes such as flash heating and melting [*Rice*, 2006]. Analyses of the fluid transport properties of exhumed fault zones show that thermal pressurization is likely to occur during large earthquakes [e.g., *Noda and Shimamoto*, 2005; *Wibberley and Shimamoto*, 2005; *Mizoguchi et al.*, 2008]. Elastohydrodynamic lubrication [*Brodsky and Kanamori*, 2001] occurs when a fluid within pore spaces in the slip zone lubricates solid-solid contacts because the viscous shear resistance of the fluid is lower than the friction between solids. During slip, the pressure of the fluids increases in response to changes in the thickness of the flow path between grains in the slip zone, supporting part of the normal stress. Both thermal pressurization and elastohydrodynamic lubrication result in a pressurized fluid phase in the slip zone. As pore fluids become pressurized, one potential product could be mobilized fault gouges or cataclasites. Evidence for mobilized cataclasite thought to be indicative of high pore fluid pressures during slip events is observed in some fault zones, primarily in the form of mesoscale veins of cataclasite injected from slip zones into adjacent wall rock [*Lin*, 1996; *Miller and Cowan*, 1998; *Cowan et al.*, 2003; *Otsuki et al.*, 2005; *Rowe et al.*, 2005; *Brodsky et al.*, 2009; *Boullier et al.*, 2009].

[11] Coseismic slip weakening may also be achieved by fluidization of granular materials whereby the bulk material achieves a fluid-like state [*Otsuki et al.*, 2003; *Lu et al.*, 2007]. Note that the presence of a fluid phase in pore spaces in the slip zone is not required for fluidization. *Otsuki et al.* [2003] suggest that transient displacement of the fault zone walls in a direction perpendicular to rupture propagation by elastic waves associated with the rupture [*Melosh*, 1996] or normal interface vibrations [*Brune et al.*, 1993] could enhance the likelihood of fluidization. Thin section evidence describing examples of fluidized active slip zones is presented for some major faults containing clay-rich gouge [e.g., *Otsuki et al.*, 2003; *Hirono et al.*, 2008], cataclasites [*Smith et al.*, 2008], and microscale analyses show that fluidization can be identified on the basis of the detection probability of fragmented counterpart particles [*Monzawa and Otsuki*, 2003].

3. Geologic Setting

[12] The left-lateral strike-slip faults examined in this study are located in two areas within the central Sierra Nevada, California: the Granite Pass region of Kings Canyon National Park, and the Bear Creek drainage in the Mount Abbot Quadrangle (Figure 1). The Sierra Nevada mountain range is composed primarily of a continuous chain of plutonic rocks that represent part of a continental magmatic arc that stretches the entire length of the west coast of North America [*Bateman*, 1992]. The faults cut granites or granodiorites analogous to the crystalline basement rocks in which many earthquakes are observed to nucleate. The majority of the faults are contained within a single pluton so do not juxtapose contrasting rock types. Where faults crosscut and displace pluton boundaries, or late stage aplite dykes, the strike-slip separation can be determined.

[13] Various lines of evidence suggest that faults in the central Sierra Nevada were active at middle to lower crustal depths. Radiometric K-Ar and ^{39}Ar-^{40}Ar dates [*Segall et al.*, 1990; *Pachell et al.*, 2003] obtained from muscovite that crystallized in faults in the central Sierra Nevada show that they were active close to the time that the host rock plutons were cooling through the biotite Ar retention temperature, i.e., ~300 to 350°C [*Evernden and Kistler*, 1970]. Depending on the geothermal gradient, these thermochronological data suggest the faults were active at depths in the region of 5 to 11 km (see *Pachell et al.* [2003] for a detailed discussion). Early ductile deformation within the faults is consistent with ambient temperatures greater than ~400°C. Ductile deformation textures are consistently crosscut by brittle fracturing and cataclasis [*Griffith et al.*, 2008; *Kirkpatrick et al.*, 2008]. Exhumation of the faults from depth in the crust has occurred without significant accompanying reactivation of the faults, which therefore preserve primary deformation textures associated with deformation at midcrustal levels.

[14] The faults in the two field areas have a range of lengths and total observed strike-slip separations. The maximum length of any of the faults is ~9 km; the corresponding largest rupture that could have occurred on the faults is M ~ 5.8 so the observations documented here are directly related to earthquakes smaller than M = 5.8 (Figure 1). In the Granite Pass area (Figure 2), we focus on the Granite Pass fault and subparallel faults defined by *Kirkpatrick et al.* [2008]. Left-lateral strike-slip separations on these faults range from ~20 to ~80 m, and lengths range from ~2 to 9 km, though the ends of the largest faults are poorly exposed so the lengths reported here are minimum estimates. In the Bear Creek area, we focus on an excellent exposure of the Seven Gables Trail fault [*Kirkpatrick et al.*, 2009] though the scarcity of offset markers in the Bear Creek area means the total displacement remains unknown. We do not intend to give an exhaustive description of the fault rocks; for further details, see *Kirkpatrick et al.* [2008, 2009].

4. Field and Microscope Observations

[15] Using the identification criteria summarized in Section 2, we use field, optical microscope and scanning

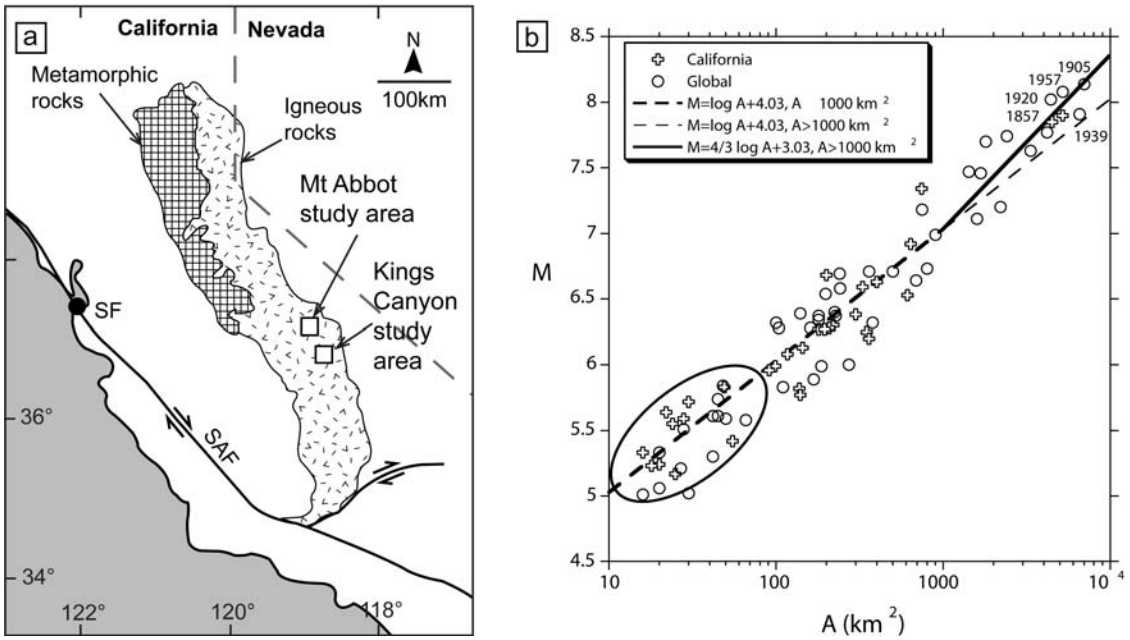

Figure 1. (a) Map showing the location of the two study areas in Sequoia and Kings Canyon National Park and the Mount Abbot Quadrangle (SF, San Francisco, SAF, San Andreas fault). (b) Graph showing the relationship between earthquake rupture area, A, and magnitude for continental strike-slip earthquakes (from *Hanks and Bakun* [2002]; data from *Wells and Coppersmith* [1994]). The ellipse indicates the range of possible earthquake magnitudes that could have occurred on the faults described in this study. Areas are calculated assuming circular ruptures occurring on faults with lengths less than the thickness of the seismogenic crust (15 to 20 km [cf. *Hanks and Bakun*, 2002]).

electron microscope (SEM) observations to investigate the slip weakening mechanisms active during ancient faulting by analyzing the deformation products they generate. Note that microscope observations are frequently required to confidently identify pseudotachylytes, but several outcrop-scale characteristics are distinctive to pseudotachylytes, allowing them to be distinguished in the field [e.g., *Kirkpatrick et al.*, 2009]. Some occurrences we report are identified on the basis of field observations alone because of sampling restrictions in the National Parks and National Forests. Following *Scholz* [2002] and *Sibson* [1977] we use the term cataclasite to refer to random fabric, brittle fault rocks. The proportion of matrix material within the rock allows a subclassification into fault breccia (10–50%), cataclasite (50–90%), and ultracataclasite (90–100%). All of the fault rocks in this study are cohesive in the terminology of *Sibson* [1977], but for brevity we will omit the term cohesive in the following rock descriptions.

[16] The faults at both sites have complex internal structures (Figure 2), characterized by one to four fault core strands containing cataclasites and ultracataclasites that crosscut early localized crystal-plastic deformation. Slip zones developed at the edges of, within and between fault cores are defined by pseudotachylytes and cataclasites with thicknesses of ~0.01 to 20 mm. Fault-related subsidiary structures are developed on either side of fault cores, defining damage zones with thicknesses of up to 30 m orthogonal to the fault. Chlorite and epidote precipitated from hydrothermal fluid flow are concentrated in fault core cataclasites and along fractures in the damage zones.

4.1. Pseudotachylytes

[17] Pseudotachylytes have recently been described from several faults in the central Sierra Nevada [*Griffith et al.*, 2008; *Kirkpatrick et al.*, 2008, 2009]. In the two study areas, we have identified pseudotachylytes in nine different faults. The pseudotachylytes generally consist of planar generation surfaces with shorter injection veins branching from the generation surfaces at high angles (Figure 3a). Generation surfaces crosscut undeformed host rock as well as cataclasites and are typically oriented subparallel to the overall fault zone trend. In some places, generation surfaces can be traced continuously along strike throughout the extent of exposure for up to around ten meters. The pseudotachylytes are up to 20 mm thick and contain cohesive, gray or black material which is often banded parallel to the vein margins in veins wider than ~5 mm. Rounded or embayed clasts within the veins are less than 3 mm long and are composed of wall rock quartz and feldspar. Interconnected, subparallel generation surfaces occasionally form networks. The generation surfaces in networks are 0.5 to 4 mm thick and are frequently curved. Some exposures contain abundant pseudotachylyte, with multiple generation surfaces that are up to 20 mm thick. Injection veins are common in these outcrops giving the host rock a brecciated appearance.

[18] Under the optical microscope, pseudotachylytes comprise dark brown or black veins that frequently have highly irregular geometries (Figure 4). Optical microscope and SEM analyses show that veins contain microcrystallites that are up to 100 μm long and around 20 μm wide.

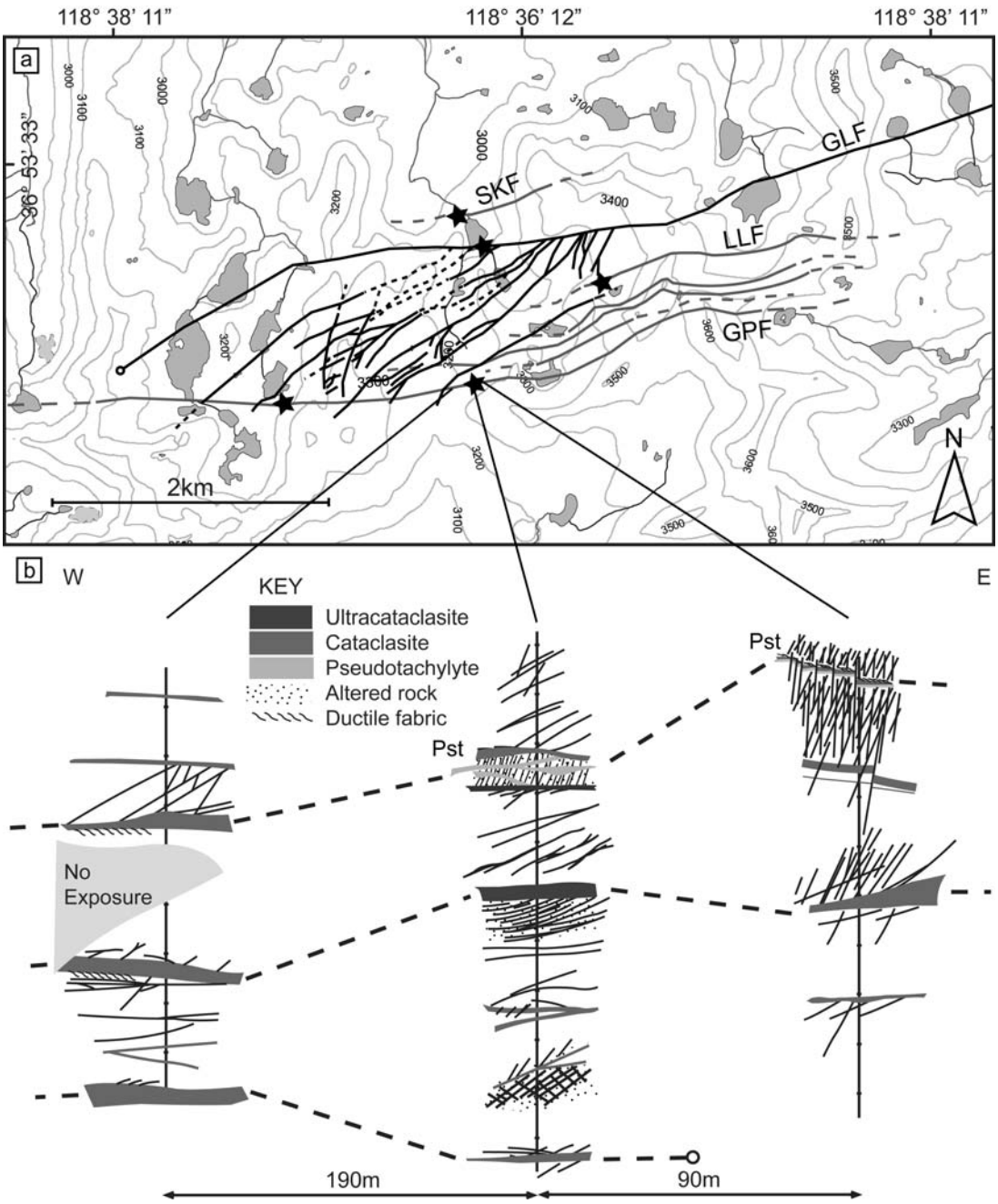

Figure 2. (a) Detailed map of the left-lateral faults in the Kings Canyon study area [from *Kirkpatrick et al.*, 2008] showing locations where pseudotachylytes have been identified (black stars). The Glacier Lakes fault and subsidiary structures (black) terminate in the region of older Granite pass faults (gray) (SKF, Skeeter fault; GLF, Glacier Lakes fault; LLF, Little Lake fault; GPF, Granite Pass fault; contours are in 100 m intervals). (b) Structural logs constructed perpendicular to the fault through three portions of the Granite Pass fault documenting its complicated internal structure and along strike variability. Ticks on vertical axes define 1 m intervals. The cataclasites and ultracataclasites define fault core strands, some of which contain pseudotachylytes (Pst), between which arrays of subsidiary faults and joints are developed (black lines). The logs are recorded qualitatively, but angular and crosscutting relationships are accurately portrayed. Three fault cores are present in the western log, which can be traced along strike to the east and correlated with the central log (dashed lines show where fault core strands are continuous). The distance between fault core strands changes along strike. Between the central and eastern logs, one of the fault cores terminates (open circle). Note that the logs are limited by the extents of the exposures at each locality.

Microcrystallites of different sizes form domains within the pseudotachylyte veins, and occasionally have aligned long axes that define flow fabrics. Microcrystallite morphologies include characteristic lath-shaped, bow-tie and sheaf-like arrangements of crystals. Close to the vein margins, all crystals are poorly developed and the vein fill is dominated

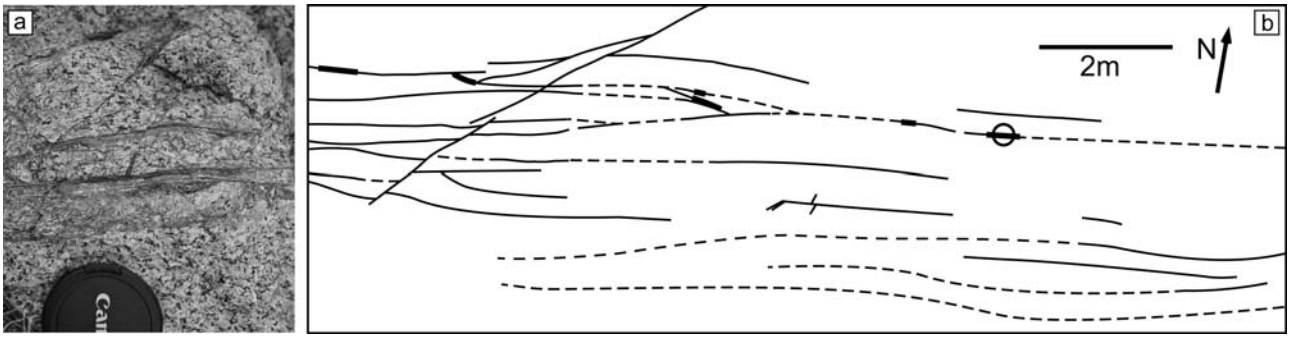

Figure 3. (a) Photograph of a pseudotachylyte generation surface and injection vein in the Seven Gables Trail fault. Camera lens for scale is ~60 mm diameter (location of photograph shown with a circle in Figure 3b). (b) Map of the fault core strands of the Seven Gables Trail fault (dashed where uncertain) and the patches of pseudotachylytes developed in the fault (heavy black lines). The pseudotachylytes are limited in lateral extent to several meters along strike. The map was constructed using the baseline mapping technique: the accuracy is ±5 cm. The fault cores are defined by the degree of grain size reduction compared to the host rock, i.e., the presence of cataclasites and ultracataclasites. Note that the internal detail of the fault cores is not discernable at the scale of this map.

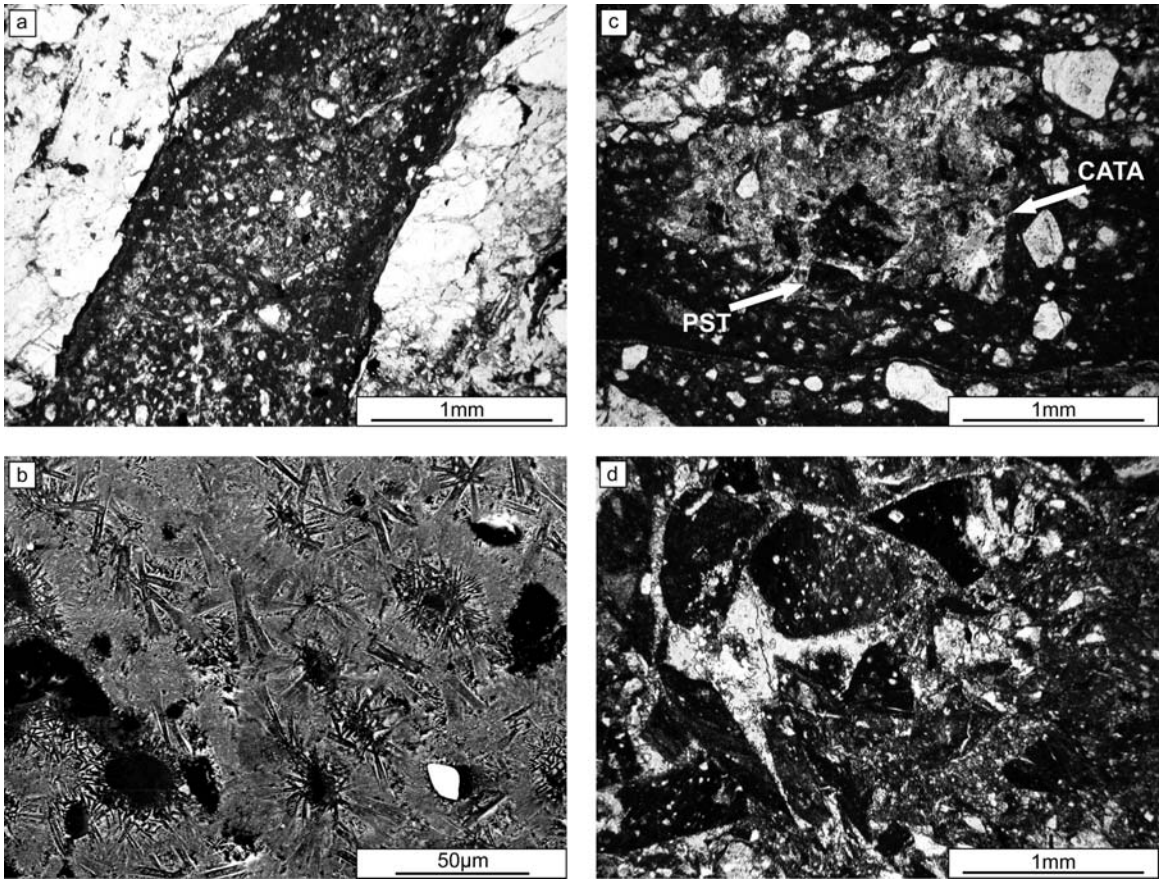

Figure 4. (a) Photomicrograph of a pseudotachylyte vein from Skeeter fault (plane polarized light). The vein has sharp edges and contains rounded and embayed lithic clasts. The vein matrix is mostly dark, cryptocrystalline material except where it is replaced with chlorite (pale gray). (b) Scanning electron microscope backscattered electron (BSE) image of pseudotachylyte from Skeeter fault. Note the sheaf-like bundles of microcrystallites. (c) A cataclasite from the Granite Pass fault with a clast (CATA) that contains a fragment of previously formed pseudotachylyte (PST, plane polarized light). (d) A pseudotachylyte vein from the Little Lake fault that has been brecciated forming large, angular fragments. The pale matrix between the fragments is chlorite (plane polarized light).

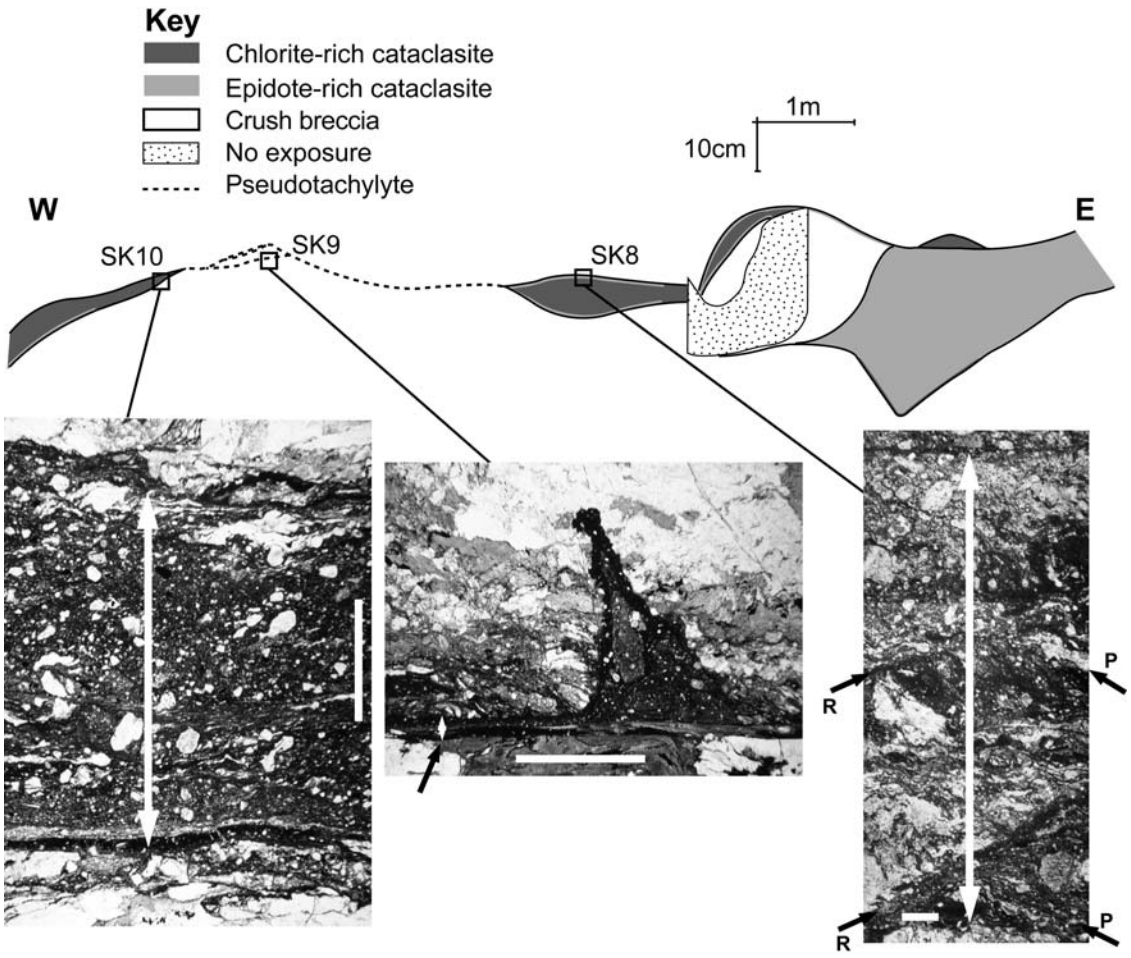

Figure 5. (top) Map showing detail of a single left-lateral fault core strand in Skeeter fault (note vertical exaggeration). The map was constructed using the baseline mapping technique; positions are accurate to ±0.5 cm. The wider parts of the fault core contain epidote- or chlorite-rich cataclasites, where the core narrows, pseudotachylytes are developed. Only one subsidiary fracture was mapped in this exposure, which is too fine to include at this scale of observation (see text for further description). (bottom) Photomicrographs of samples collected from along the fault core strand (plane polarized light, scale bars are 1 mm in all cases). Sample SK10 contains a random fabric cataclasite, sample SK9 is crosscut by a pseudotachylyte generation surface (injection vein also shown), and SK8 contains a foliated cataclasite (orientations of the foliations correspond to the P and R Riedel shear orientations as indicated). In all images the white bar represents 1 mm, and the white arrow delimits the width of the inferred slip zone. A black arrow highlights the representative thickness of the narrow pseudotachylyte generation surface in SK9 (center).

by cryptocrystalline material. Sulphide and titanite droplets (identified by energy dispersive X-ray spectroscopy) are common in the pseudotachylyte veins. Vesicles (indicative of pseudotachylyte generation at shallow depths) are not observed. Some pseudotachylyte veins are altered, or replaced with granular chlorite and epidote. Fault rock samples from the Granite Pass faults contain brecciated pseudotachylytes, and fragments of pseudotachylyte are frequently found as reworked clasts within cataclasites (Figure 4). Such pseudotachylyte clasts are often rounded, altered and are crosscut by veins containing quartz or chlorite.

[19] Pseudotachylyte generation surfaces are developed in patches up to 4 m long along well-exposed portions of the Seven Gables Trail fault (Figure 3) and Skeeter fault (Figure 5). The Seven Gables Trail fault has a complex internal structure consisting of several anastomosing fault core strands. Within the fault core strands pseudotachylytes are developed in patches adjacent to cataclasites that display no evidence for melting. The longest observed patch is developed along one of the fault core strands of the Skeeter fault and is 4 m long. The thickness of this fault core strand changes from ~35 to ~2 cm within 10 m along strike (Figure 5). The fault core is flanked on either side by zones of altered host rock ~10 cm wide in which biotite and hornblende are chloritized, indicating microscale damage. Only one subsidiary fracture was identified in the mapped exposure. This fracture is ~0.8 m long with an aperture of much less than 1 mm and branches several times in a direction away from the fault core strand. Microscope analyses of samples from the Skeeter fault core confirm that pseudotachylyte is present in the narrow part of the

Figure 6. Photograph of a typical fault core strand in the Granite Pass fault containing juxtaposed cataclasites (midgray) and ultracataclasites (black). Compass for scale is 10 cm long.

strand. The pseudotachylyte defines a slip zone with a thickness up to 0.25 mm and is not itself deformed so must have been generated in the most recent increment of slip on the strand. In the adjacent, wider, parts of the fault core foliated and nonfoliated cataclasites are developed. Thin section scale crosscutting relations suggest that the most recent increment of slip in the cataclastic parts of the fault core was localized onto zones 13 and 4 mm thick within the cataclasites. Hydrothermal chlorite and epidote are more abundant in the wider parts of the fault core, in particular epidote comprises a large proportion of the cataclasites, but are limited in the narrow part of the fault core.

4.2. Cataclasites

[20] Brittle fault rocks in the Sierra Nevada faults range in their degree of comminution from fault breccias to cataclasites and ultracataclasites. Fault rocks are developed in strands that delimit the most intensely deformed parts of the faults, the fault cores. Fault cores frequently contain juxtaposed fault breccias, cataclasites and ultracataclasites with crosscutting relations consistently showing that the most comminuted unit is the most recent (Figure 6). The edges of fault core strands are typically sharp but have irregular geometries, so order of magnitude thickness changes frequently occur within tens of meters along strike.

[21] Optical microscope and SEM analysis of the brittle fault rocks shows that they are composed of fragments of unaltered host rock minerals (quartz, plagioclase, alkali feldspar and occasional biotite and hornblende) and also hydrothermal chlorite and epidote (Figures 5, 6, 7, and 8). Fault breccias typically contain wall rock fragments in which the igneous texture of the host granodiorite remains intact. Biotite and hornblende are frequently chloritized in the breccias and cataclasites, and chlorite is abundant in pervasive intergranular and intragranular fractures. Cataclasites mostly have random fabric and comprise angular to rounded clasts that are fragments of host rock minerals or previously formed cataclasites. Occasionally, foliated cataclasites can be identified where ordered sets of slip zones correspond to Riedel shear orientations consistent with left-lateral slip on the fault (e.g., Figure 5). Matrix material in the cataclasites is chlorite, epidote, a mix of the two, and may also include finely comminuted host rock fragments. Ultracataclasites are more comminuted than cataclasites. The ultracataclasites comprise up to ~90% matrix material consisting predominantly of granular (~10 μm) chlorite and epidote surrounding rounded quartz and alkali feldspar clasts (Figure 7). Quartz-filled veins crosscut ultracataclasites and are variably deformed, showing that fracturing and hydrothermal fluid migration required to form the quartz veins were coeval with cataclasis.

[22] The Granite Pass fault contains evidence for mobilization of cataclasite. Juxtaposed cataclasites and ultra-

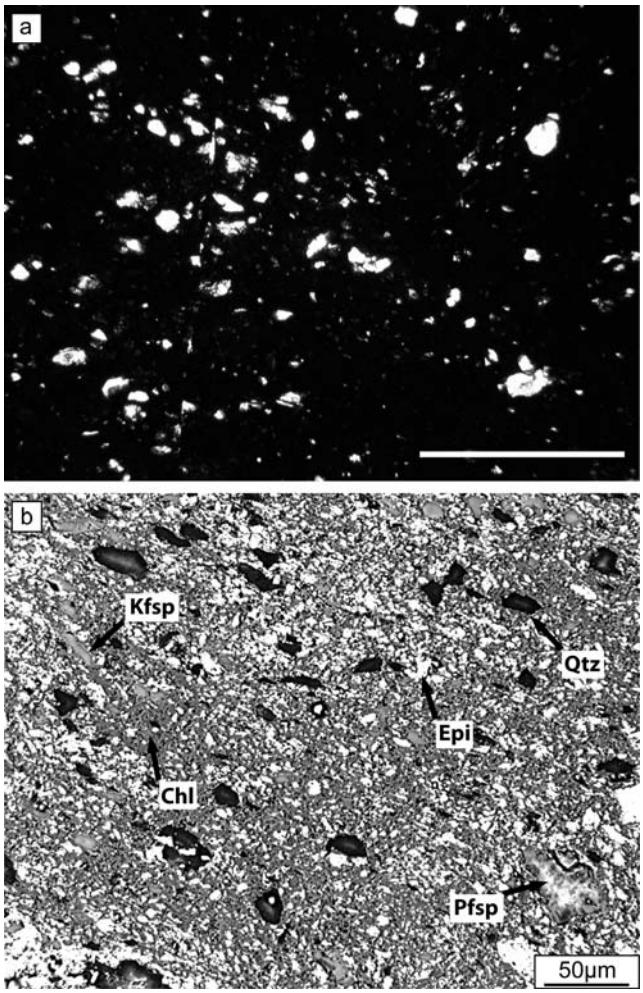

Figure 7. (a) Photomicrograph (plane polarized light) of a typical ultracataclasite from the GPF. Rounded clasts of quartz and alkali feldspar are present in an aphanitic matrix (which appears dark in thin section because it is so fine grained) than can comprise up to ~90% of the ultracataclasite (scale bar 1 mm). (b) SEM backscattered electron (BSE) image of part of the matrix from the same ultracataclasite sample as in a. Fragment compositions (Qtz, quartz; Kfsp, alkali feldspar; Pfsp, plagioclase feldspar; Epi, epidote; Chl, chlorite) are assessed using energy dispersive X-ray spectroscopy (EDS). The composition of the ultracataclasite matrix (chlorite 47%, epidote 37%, quartz 11%, alkali feldspar 4%, plagioclase, titanite and other metal oxides ~1%) was assessed by point counting.

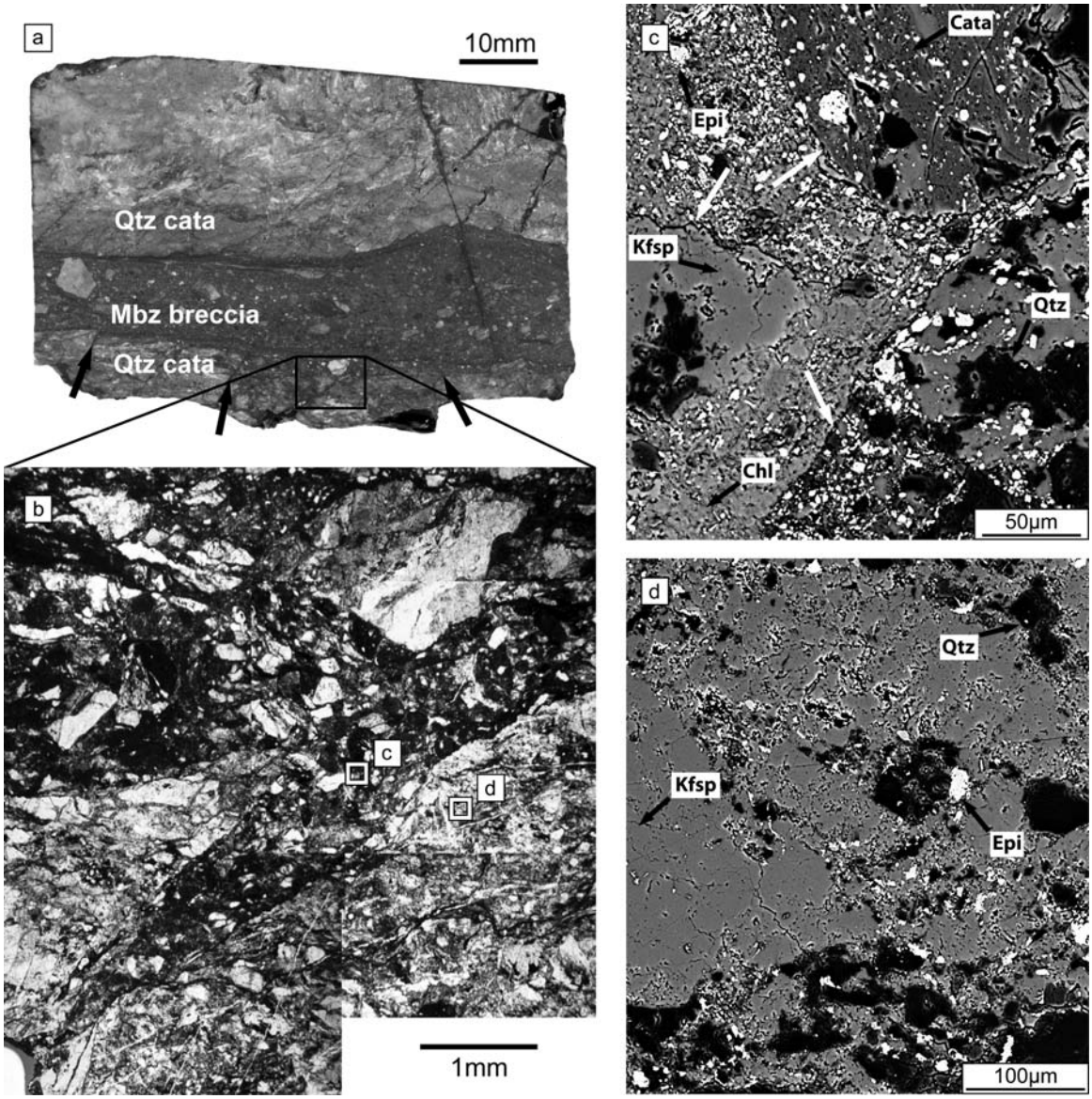

Figure 8. (a) Photograph of a polished sample of cataclasite from the Granite Pass fault from which a thin section was prepared for microscope and SEM analyses. The oriented sample is cut perpendicular to the fault and contains the slip vector (assumed horizontal for a strike-slip fault [cf. *Kirkpatrick et al.*, 2008]). Two different rock types are discernable, which are identified from microscope observations as quartz- and alkali feldspar-rich cataclasites (Qtz cataclasite) and a mobilized breccia (Mbz breccia). Black arrows indicate the locations of geometric irregularities in the breccia-cataclasite boundary that are filled with breccia. (b) Montage of photomicrographs of the oriented sample showing a mobilized fault breccia in the Granite Pass fault (plane polarized light). The mobilized breccia is in the upper part of the image and contains angular clasts up to 2.3 mm long. The breccia clasts contain a higher proportion of dark material (often pseudotachylyte fragments) than the adjacent quartz-rich cataclasite in the lower part of the image. A fracture with a geometry similar to an injection vein can be seen cutting the quartz-rich cataclasite, extending to the lower left corner of the image. Similar structures can be seen along the boundary between mobilized breccia and the lower quartz-rich cataclasite at the arrows in Figure 8a. The breccia material is the same in the fracture and the main breccia domain. Boxes show the locations of Figures 8c and 8d. (c) Scanning electron microscope BSE image of the mobilized breccia showing clasts of varied compositions in a chlorite-rich matrix. Clast boundaries are shown by white arrows (labels as in Figure 7, except for Cata which is a previously formed cataclasite). (d) BSE image of the quartz cataclasite showing the more uniform composition of the cataclasite and lack of matrix compared to the breccia (labels as in Figure 7).

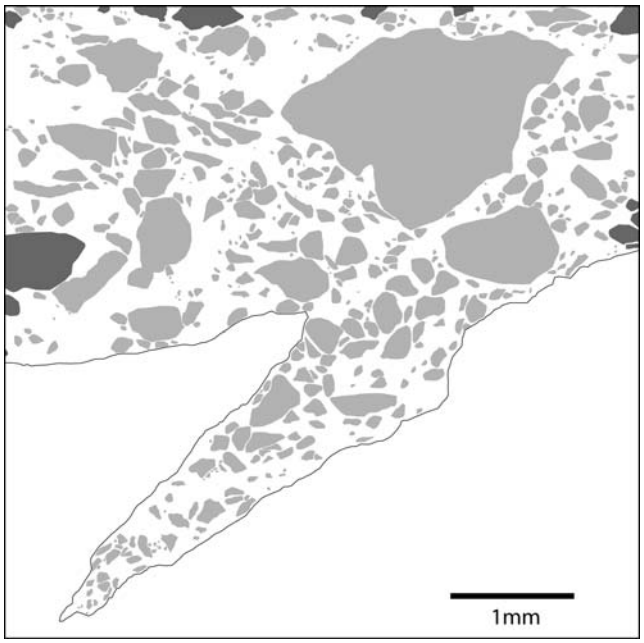

Figure 9. Clasts in the mobilized breccia, defined by optical microscope analysis of the image in Figure 8b at 100x magnification, show continuous texture of the mobilized breccia into the injection vein. All visible clasts at this scale of observation are shown; clast long axes are 0.01 to 2.3 mm. The dark gray clasts are those that extend beyond the area analyzed (shown by back bounding box).

cataclasites are evident in exposure (Figure 6), but distinctive injection vein-like structures have not been identified at the outcrop scale. In thin section, one fault core sample contains a random fabric fault breccia consisting of ~53% angular to rounded clasts in a chlorite-rich matrix (Figure 8). The clasts are 0.01 to 2.3 mm long and have a variety of compositions including fragments of previously formed cataclasite, pieces of pseudotachylyte, fragments of quartz veins, and occasional fragments of wall rock quartz, plagioclase and alkali feldspar. The matrix is almost exclusively composed of chlorite grains ($\leq$0.01 mm diameter), which have a hydrothermal origin. The fault breccia crosscuts a quartz- and alkali feldspar-rich cataclasite in which fragments are smaller ($\leq$0.8 mm), more rounded and contain pronounced crystal-plastic deformation textures. Chlorite and epidote are rare in the cataclasite, which is clast-supported at all observed scales up to ~1000$\times$ magnification (Figure 8).

[23] The boundary between the fault breccia and quartz cataclasite domain is clear under the microscope. The main breccia domain is oriented subparallel to the macroscale fault zone. A fracture filled with the same breccia material branches from the main breccia domain with an injection vein-like geometry (Figure 8). Crosscut clasts in the adjacent quartz cataclasite show that the fault breccia has 'intruded' into the cataclasite. Although the breccia-filled fracture has a similar orientation to Riedel shears observed in other sampled cataclasites (e.g., Figure 5), those Riedel shears are defined by extremely fine, comminuted shear planes crosscutting the cataclasite, rather than breccia. Several similar, though smaller, irregularities in the boundary between the fault breccia and quartz-rich cataclasite can be seen in hand specimen. In each case, the irregularities are filled with the fault breccia. The continuity of the breccia composition into the fracture shows that the breccia filled the fracture during the same deformation event that formed the breccia (Figure 9). If the fracture had formed later than the breccia, then by comparison with other samples, the fracture would be filled with chlorite only (see Figure 4d). Analogous intrusive fault gouges and cataclasites filling injection veins and other geometric irregularities have also been interpreted as being indications that the gouge was mobilized [e.g., *Cowan et al.*, 2003; *Otsuki et al.*, 2005; *Rowe et al.*, 2005].

5. Interpreted Slip-Weakening Mechanisms

[24] Field and microscope observations should be useful for inferring the active slip weakening mechanisms during ancient earthquakes if deformation products of the mechanisms are preserved in fault rocks (section 2). Our results show that pseudotachylytes are often preserved in the Sierra Nevada faults, indicating that melt lubrication may have been a significant processes. The presence of discontinuous pseudotachylytes could result in increases in dynamic shear resistance causing velocity strengthening rather than slip weakening by melt lubrication [*Fialko and Khazan*, 2005; *Hirose and Shimamoto*, 2005]. However, in some instances individual pseudotachylyte generation surfaces can be traced throughout the extent of exposure indicating continuous lengths of over ten meters. The abundance, lengths and thicknesses of these throughgoing pseudotachylytes suggests that frictional melting was likely to have weakened the faults during coseismic slip [*Di Toro et al.*, 2006]. It is not possible to obtain an independent estimate of stress drop for the pseudotachylyte-bearing faults we study, so the lubrication effect of the melts remains somewhat speculative. Estimates of stress drops from field observations of exceptional exposures of nearby small displacement faults in the Sierra Nevada by *Griffith et al.* [2009] show that cataclasite bearing faults with no pseudotachylytes experienced large (90–250 MPa) stress drops. Similar magnitude stress drops on the faults in our study area would imply that the faults weakened during coseismic slip, even where continuous pseudotachylytes are absent.

[25] Cataclasites are common in all of the faults, the majority of which do not contain obvious evidence for slip weakening mechanisms, or more generally seismic slip. However, fault breccia filling several injection vein-like structures (Figure 8) appears to have been mobilized during deformation. This fault rock is texturally different to the adjacent cataclasites as it is matrix-supported with chlorite forming a fine-grained matrix (Figure 9). The adjacent cataclasite is clast-supported, and does not contain an identifiable matrix. The clasts in the cataclasite are dominated by quartz and alkali feldspar, contrasting with the diverse range of clast types in the breccia. The 'intrusive' nature of the breccia, which is texturally continuous into the injection, indicates that the breccia was mobilized during the deformation event that formed the breccia.

[26] As discussed in Section 2, mobilization of brittle fault rocks is one potential indicator of pressurization as a

result of thermal pressurization or elastohydrodynamic lubrication. Given that pseudotachylytes in these faults attest to seismic slip rates, the mobilized breccia may represent the product of one of these weakening mechanisms. Chlorite is the major constituent of the matrix in the breccia, suggesting that hydrothermal fluids were either present during coseismic slip or at some time afterwards. If the breccia formed in the absence of a free fluid phase, the chlorite could subsequently have filled porosity induced by cataclastic dilation after slip had finished. However, microscope and SEM analyses of the breccia show that it is matrix-supported, indicating that the matrix formed at the same time as the clasts. Chlorite could also have replaced an original matrix material formed exclusively from comminution of the host rock, though such replacement would effect the clasts as well, which has not occurred. The textural observations suggest that a coseismic hydrothermal fluid was present in the breccia at the time it formed. Pressurization of the hydrothermal fluid is the best explanation for the mobilization of the breccia. The fault breccia and injection vein therefore potentially represent the products of processes such as thermal pressurization or elastohydrodynamic lubrication, although it is not possible to distinguish the two.

[27] The outcrop-scale distribution of deformation products in the faults shows that multiple processes were active synchronously along strike during a single rupture event. In the Skeeter fault and Seven Gables Trail fault, pseudotachylytes are limited in lateral extent to several meters along strike, and are developed between cataclasite-rich fault cores that do not contain obvious evidence for seismic slip. The pseudotachylytes could potentially have formed during tiny earthquakes, with rupture lengths approximately equal to the patch lengths. Following *Sibson* [2003], the temperature rise, ΔT, for uniform adiabatic shearing in a slip zone of width t_s is given by

$$\Delta T = \frac{\tau_f . u}{c_p . \rho . t_s} (^\circ\mathrm{C}), \quad (1)$$

where τ_f is the shear resistance (assumed to be constant) during a slip increment u, ρ is the rock density, c_p is the specific heat. If the coseismic slip is $\sim 10^4$ times smaller than the rupture length [*Scholz*, 2002], the slip in earthquake with a rupture length of 4 m (the length of the pseudotachylyte patch in the Skeeter fault) would be u = 0.0004 m. Assuming a coefficient of friction of 0.6 and that the normal stress acting on the fault is lithostatic, then at the maximum likely depth of fault slip, 11 km, τ_f is ~170 MPa. Using c_p = 1000 J/kg °C [*Sibson*, 2003] and ρ = 2500 kg/m^3, the temperature rise, ΔT is ~109°C for t_s = 0.25 mm, which is insufficient to melt any of the minerals in the host rock even at the elevated temperatures likely at the depths these faults were slipping at (~240°C at 8 km for a geothermal gradient of 30°C/km). This simple analysis shows that pseudotachylytes must have formed during small earthquakes that ruptured areas greater than the length of the pseudotachylytes. The distribution of pseudotachylytes in the fault shows that melt lubrication can only have been an active slip weakening mechanism over part of the rupture surface. Similar patches of pseudotachylyte in the Granite Pass fault and other faults show that the frictional response to slip was commonly spatially variable on these faults.

[28] One exposure of the Skeeter fault demonstrates that slip zone thickness, and more generally fault structure, appears to control which process is active at a point along the fault. The northern fault core strand of Skeeter fault contains a pseudotachylyte generation surface that is ~4 m long (Figure 5). The pseudotachylyte is not subsequently deformed, and so must have formed during the most recent slip increment along this part of the fault. The slip zone thickness defined by the pseudotachylytes in the narrow part of the fault core is less than 0.25 mm. In the adjacent, wider parts of the fault core, the last increment of slip appears to be localized onto zones 4 to 13 mm thick within cataclastic fault rocks that do not contain evidence of frictional melting. More generally, the cataclasites do not contain obvious evidence for seismicity, showing that identifying slip weakening mechanisms in cataclasites elsewhere is likely to be extremely difficult. The deformation product along the fault core strand, and by inference the coseismic frictional response of the fault, varies along strike for a single rupture event, and correlates with slip zone thickness. *Griffith et al.* [2008] also noted melting was restricted to the narrowest slip zones in other faults in the central Sierra Nevada. Multiple noncoplanar pseudotachylyte generation surfaces have been observed at several localities along the Granite Pass fault, demonstrating that the spatial distribution of the pseudotachylytes with respect to the mesoscale fault architecture is complex.

[29] There is also evidence that the slip weakening mechanism may change through time at an individual point along the fault. Fault rock samples in the Little Lake and Granite Pass faults frequently contain reworked and fragmented pseudotachylytes (Figure 4). If these fragmented pseudotachylyte veins were deformed in response to seismic slip, the slip weakening mechanism must have changed at a point on the fault from melt lubrication (at the time the pseudotachylytes formed) to something else. *Sibson* [1973] suggested that melt generation is limited to incipient structures in which low fault permeability restricts the potential for fault-hosted fluids to decrease the effective normal stress across the slipping zone (i.e., thermal pressurization is inhibited). Reworked pseudotachylyte material in the Granite Pass fault in particular is evidence for repeated pseudotachylyte generation and repeated seismic slip events. Evidence for syndeformation fluid-related alteration is present in the form of chlorite and epidote mineralization in the matrix of the cataclasites, some of which were subsequently crosscut by pseudotachylytes. Fluids were therefore present in the faults before, after, and potentially during slip events. That the fluids did not preclude melt generation suggests either that no free fluid phase was present at the onset of slip, or that competition between weakening mechanisms is inherent in the frictional response to slip and that the conditions in the slip zone dictate which mechanism prevails.

6. Discussion

[30] The exhumed faults in the Sierra Nevada are analogs for modern tectonically active faults as they have been exhumed from seismogenic depths without significant associated deformation. Our results demonstrate that these faults contain evidence for multiple slip weakening mechanisms during faulting as well as spatially variable coseis-

mic processes and frictional response to slip during a single rupture. The microstructures used to define melt lubrication and a pressurization mechanism define slip zones with thicknesses of 0.01 to 25 mm from pseudotachylytes and up to 20 mm for mobilized fault breccias within cataclastic fault cores. *Cocco and Tinti* [2008, p. 125] point out that the seismologically derived slip weakening model is a description of the macroscopic behavior of an entire rupture and argue that it cannot ''distinguish the diverse physical processes acting at the micro- and meso-scale within the fault zone'' (length scales from millimeters to hundreds of meters). The observations we present emphasize that macroscopic dynamic fault weakening is a function of multiple coeval processes at the microscale to mesoscale, which cannot be distinguished by seismological techniques.

[31] Dynamic rupture simulations show that the frictional response of a fault to slip is inherently related to stress drop, slip magnitude and slip velocity. However, several studies also demonstrate that matching strong motion data with rupture simulations cannot resolve both the stress drop and slip weakening distance [e.g., *Guatteri and Spudich*, 2000; *Peyrat et al.*, 2004]. The mixed deformation products of seismic slip that we document suggest that both spatially variable slip weakening distance and dynamic shear resistance may be expected during coseismic slip. Though the geologic observations are at a small scale compared to the macroscopic seismic source, this interpretation is in agreement with inversions of seismic data that suggest D_c is spatially variable [*Ide and Takeo*, 1997]. The rheology of a fault is impossible to define from observations of the fault rock assemblage alone, but the implications of spatially varying dynamic weakening processes can be qualitatively assessed for various source parameters if the traction evolution is different for different active processes. Stress drop corresponds to slip magnitude [*Aagaard and Heaton*, 2008] so the slip distribution during the earthquakes on the Sierra Nevada faults was probably heterogeneous. Additionally, numerical simulations show that spatially variable D_c can cause changes in slip velocity and ultimately arrest rupture propagation [*Guatteri and Spudich*, 2000]. The overall implications of the geologic observations are consistent with finite source inversions of strong ground motion data, which frequently show that source parameters such as static stress drops, slip magnitudes and dislocation rise times are vary across a rupture surface [e.g., *Beroza and Mikumo* 1996].

[32] Geologic observations provide an opportunity to infer the distribution of yield stress, τ_y, from the deformation products within fault zones. In the case of the Sierra Nevada faults, the deformation products in the slip zones and fault cores are spatially variable as a result of varying coseismic processes. The deformation products themselves likely have differing yield strengths. Recent studies of pseudotachylytes that decorate large proportions of faults in the Gole Larghe fault zone, Italy, suggest that pseudotachylyte generation effectively locks a fault by fusing the opposing wall rocks with molten material [*Di Toro and Pennacchioni*, 2005]. Pseudotachylyte generation in those faults caused the faults to ''lock up'' and slip to transfer to adjacent structures. In the Sierra Nevada faults, pseudotachylytes have a patchy distribution, so likely result in regions of higher yield stress on the faults compared to adjacent chlorite- and epidote-rich cataclasites and ultracataclasites. Healing processes and rates are also probably different for friction-induced melts and mobilized breccias; quenching of melts likely occurs within seconds of rupture arrest [*Di Toro and Pennacchioni*, 2004], whereas cementation of the breccias with chlorite could occur over days or years [e.g., *Olsen et al.*, 1998]. Furthermore, for an initially uniform stress distribution, if melt lubrication and a pressurization slip weakening mechanism are characterized by different τ_f and stress drop, the spatial distribution of deformation products could lead to spatially variable postrupture shear stress. Geologic evidence therefore supports the inference of *Rivera and Kanamori* [2002] that shear stress distribution as well as friction is spatially heterogeneous.

[33] The coseismic processes active in the slip zone in the Sierra Nevada faults appear to be controlled by the structure of the fault zone, and in particular the thickness of the slip zone. Experimental [e.g., *Marone and Kilgore*, 1993] and theoretical [e.g., *Brodsky and Kanamori*, 2001; *Rice*, 2006] studies demonstrate that thickness of the slip zone is a critical parameter to the slip weakening behavior. Fault zones with varying internal structure should therefore be expected to demonstrate complex frictional behavior. The Sierra Nevada faults are relatively immature structures (total slip <100 m) compared to many of the faults that make up plate boundary systems. Scaling relations suggest that the largest earthquake that could have occurred on the studied faults would have been $M_w \sim 5.8$ (Figure 1), implying that the frictional behavior for ancient earthquakes interpreted from the faults would correspond to small to moderate sized events. Some exposures of mature faults, for example the Punchbowl fault, suggest that they have characteristically simple internal structures [e.g., *Chester and Chester*, 1998]. However, natural faults are widely known to involve bends and step overs that strongly influence rupture propagation [e.g., *King and Nabelek*, 1985; *Wesnousky*, 2006]. Recent studies have also revealed that mature faults including the Punchbowl fault [*Schulz and Evans*, 2000], San Andreas fault [*Dor et al.*, 2006], Chelungpu fault [*Heermance et al.*, 2003; *Boullier et al.*, 2009] and the Nojima fault [e.g., *Mizoguchi et al.*, 2008] do contain along-strike variability in their internal structure. These faults have accumulated kilometers of displacement, suggesting that geologic heterogeneity is present over a wide range of scales in mature faults.

7. Conclusions

[34] Faults exhumed from seismogenic depths in the central Sierra Nevada, California, contain evidence for multiple slip weakening mechanisms during ancient earthquake ruptures. Pseudotachylytes attest to slip at seismic slip rates, and where continuous likely represent melt lubrication. Mobilized and chloritized fault breccias are indicative of pressurized coseismic fluids that could have resulted from either thermal pressurization and/or elastohydrodynamic lubrication. Energy considerations show pseudotachylytes that developed in patches several meters long must have formed during ruptures larger than the patch sizes, implying that cataclasites adjacent to the patches also localized seismic slip. The distribution of the deformation products in the faults shows that the coseismic processes, and by inference the frictional response to slip, during a

single rupture event are spatially variable, and also that the active slip weakening mechanism at a point on the fault can change over time. Geologic evidence therefore emphasizes that macroscopic dynamic weakening is a function of multiple coeval processes at microscales and mesoscales. Combined field and microscope observations suggest that fault zone structure, and particularly the width of the slip zone, controls which processes are activated during slip. Along-strike changes in the slip zone thickness indicate that the frictional response to slip that occurred on the Sierra Nevada faults was characterized by spatially variable source parameters such as slip weakening distance, dynamic frictional strength, stress drop and slip magnitude. By analogy, heterogeneous friction may be expected during slip on tectonically active faults. Our results emphasize that the frictional response of a fault to slip is dependent on the internal structure of faults and that given the along-strike heterogeneity of most mapped fault zones, the coexistence of multiple slip weakening mechanisms in a single earthquake will be common.

[35] **Acknowledgments.** We thank Jim Evans and Aderson do Nascimento for discussion and comments that helped formulate this manuscript. Reviews by Giulio Di Toro and Darrel Cowan greatly improved the manuscript. J.D.K. was supported by a Natural Environment Research Council grant (NE/E005365/1). John Gilleece and Peter Chung are thanked for sample preparation and help with SEM analyses. Thanks to the National Park Service and National Forest Service for fieldwork and sampling permits.

References

Aagaard, B. T., and T. H. Heaton (2008), Constraining fault constitutive behavior with slip and stress heterogeneity, *J. Geophys. Res.*, *113*, B04301, doi:10.1029/2006JB004793.

Andrews, D. J. (1976), Rupture propagation with finite stress in antiplane strain, *J. Geophys. Res.*, *81*(20), 3575–3582, doi:10.1029/JB081i020p03575.

Aochi, H., and S. Ide (2009), Complexity in earthquake sequences controlled by multiscale heterogeneity in fault fracture energy, *J. Geophys. Res.*, *114*, B03305, doi:10.1029/2008JB006034.

Barker, S. L. L. (2005), Pseudotachylyte-generating faults in central Otago, New Zealand, *Tectonophysics*, *397*(3–4), 211–223, doi:10.1016/j.tecto.2004.12.005.

Bateman, P. C. (1992), Plutonism in the central part of the Sierra Nevada batholith, California, *U.S. Geol. Surv. Prof. Pap.*, *1483*, 186 pp.

Beeler, N. M., T. E. Tullis, and D. L. Goldsby (2008), Constitutive relationships and physical basis of fault strength due to flash heating, *J. Geophys. Res.*, *113*, B01401, doi:10.1029/2007JB004988.

Beroza, G. C., and T. Mikumo (1996), Short slip duration in dynamic rupture in the presence of heterogeneous fault properties, *J. Geophys. Res.*, *101*(B10), 22,449–22,460, doi:10.1029/96JB02291.

Beroza, G. C., and P. Spudich (1988), Linearized inversion for fault rupture behavior: Application to the 1984 Morgan Hill, California, earthquake, *J. Geophys. Res.*, *93*(B6), 6275–6296, doi:10.1029/JB093iB06p06275.

Bouchon, M., H. Sekiguchi, K. Irikura, and T. Iwata (1998), Some characteristics of the stress field of the 1995 Hyogo-Ken Nanbu (Kobe) earthquake, *J. Geophys. Res.*, *103*(B10), 24,271–24,282, doi:10.1029/98JB02136.

Boullier, A.-M., E.-C. Yeh, S. Boutareaud, S.-R. Song, and C.-H. Tsai (2009), Microscale anatomy of the 1999 Chi-Chi earthquake fault zone, *Geochem. Geophys. Geosyst.*, *10*, Q03016, doi:10.1029/2008GC002252.

Brodsky, E. E., and H. Kanamori (2001), Elastohydrodynamic lubrication of faults, *J. Geophys. Res.*, *106*(B8), 16,357–16,374, doi:10.1029/2001JB000430.

Brodsky, E. E., C. D. Rowe, F. Meneghini, and J. C. Moore (2009), A geological fingerprint of low-viscosity fault fluids mobilized during an earthquake, *J. Geophys. Res.*, *114*, B01303, doi:10.1029/2008JB005633.

Brune, J. N., S. Brown, and P. A. Johnson (1993), Rupture mechanism and interface separation in foam rubber models of earthquakes: A possible solution to the heat-flow paradox and the paradox of large overthrusts, *Tectonophysics*, *218*(1–3), 59–67, doi:10.1016/0040-1951(93)90259-M.

Chester, F. M., and J. S. Chester (1998), Ultracataclasite structure and friction processes of the Punchbowl fault, San Andreas system, California, *Tectonophysics*, *295*(1–2), 199–221, doi:10.1016/S0040-1951(98)00121-8.

Cocco, M., and E. Tinti (2008), Scale dependence in the dynamics of earthquake propagation: Evidence from seismological and geological observations, *Earth Planet. Sci. Lett.*, *273*, 123–131, doi:10.1016/j.epsl.2008.06.025.

Cohee, B. P., and G. C. Beroza (1994), Slip distribution of the 1992 Landers earthquake and its implications for earthquake source mechanics, *Bull. Seismol. Soc. Am.*, *84*(3), 692–712.

Cowan, D. S. (1999), Do faults preserve a record of seismic slip? A field geologist's opinion, *J. Struct. Geol.*, *21*(8–9), 995–1001, doi:10.1016/S0191-8141(99)00046-2.

Cowan, D. S., T. T. Cladouhos, and J. K. Morgan (2003), Structural geology and kinematic history of rocks formed along low-angle normal faults, Death Valley, California, *Geol. Soc. Am. Bull.*, *115*, 1230–1248, doi:10.1130/B25245.1.

Das, S., and K. Aki (1977), Fault plane with barriers: Versatile earthquake model, *J. Geophys. Res.*, *82*(36), 5658–5670, doi:10.1029/JB082i036p05658.

Di Toro, G., and G. Pennacchioni (2004), Superheated friction-induced melts in zoned pseudotachylytes within the Adamello tonalites (Italian southern Alps), *J. Struct. Geol.*, *26*(10), 1783–1801, doi:10.1016/j.jsg.2004.03.001.

Di Toro, G., and G. Pennacchioni (2005), Fault plane processes and mesoscopic structure of a strong-type seismogenic fault in tonalites (Adamello batholith, southern Alps), *Tectonophysics*, *402*(1–4), 55–80, doi:10.1016/j.tecto.2004.12.036.

Di Toro, G., D. L. Goldsby, and T. E. Tullis (2004), Friction falls towards zero in quartz rock as slip velocity approaches seismic rates, *Nature*, *427*(6973), 436–439, doi:10.1038/nature02249.

Di Toro, G., G. Pennacchioni, and G. Teza (2005a), Can pseudotachylytes be used to infer earthquake source parameters? An example of limitations in the study of exhumed faults, *Tectonophysics*, *402*(1–4), 3–20, doi:10.1016/j.tecto.2004.10.014.

Di Toro, G., S. Nielsen, and G. Pennacchioni (2005b), Earthquake rupture dynamics frozen in exhumed ancient faults, *Nature*, *436*(7053), 1009–1012, doi:10.1038/nature03910.

Di Toro, G., T. Hirose, S. Nielsen, G. Pennacchioni, and T. Shimamoto (2006), Natural and experimental evidence of melt lubrication of faults during earthquakes, *Science*, *311*(5761), 647–649, doi:10.1126/science.1121012.

Dor, O., Y. Ben-Zion, T. K. Rockwell, and J. Brune (2006), Pulverized rocks in the Mojave section of the San Andreas fault zone, *Earth Planet. Sci. Lett.*, *245*(3–4), 642–654, doi:10.1016/j.epsl.2006.03.034.

Evans, J. P. (1990), Textures, deformation mechanisms, and the role of fluids in the cataclastic deformation of granitic rocks, in *Deformation Mechanisms, Rheology and Tectonics*, edited by R. J. Knipe and E. H. Rutter, *Geol. Soc. London Spec. Publ.*, *54*, 29–39.

Evernden, J. F., and R. W. Kistler (1970), Chronology of emplacement of Mesozoic batholithic complexes in California and western Nevada, *U.S. Geol. Surv. Prof. Pap.*, *632*, 42 pp.

Faulkner, D. R., A. C. Lewis, and E. H. Rutter (2003), On the internal structure and mechanics of large strike-slip fault zones: Field observations of the Carboneras fault in southeastern Spain, *Tectonophysics*, *367*(3–4), 235–251, doi:10.1016/S0040-1951(03)00134-3.

Fialko, Y., and Y. Khazan (2005), Fusion by earthquake fault friction: Stick or slip?, *J. Geophys. Res.*, *110*, B12407, doi:10.1029/2005JB003869.

Griffith, W. A., G. di Toro, G. Pennacchioni, and D. D. Pollard (2008), Thin pseudotachylytes in faults of the Mt. Abbot quadrangle, Sierra Nevada: Physical constraints for small seismic slip events, *J. Struct. Geol.*, *30*(9), 1086–1094, doi:10.1016/j.jsg.2008.05.003.

Griffith, W. A., G. Di Toro, G. Pennacchioni, D. D. Pollard, and S. Nielsen (2009), Static stress drop associated with brittle slip events on exhumed faults, *J. Geophys. Res.*, *114*, B02402, doi:10.1029/2008JB005879.

Guatteri, M., and P. Spudich (2000), What can strong-motion data tell us about slip-weakening fault-friction laws?, *Bull. Seismol. Soc. Am.*, *90*(1), 98–116, doi:10.1785/0119990053.

Hanks, T. C., and W. H. Bakun (2002), A bilinear source-scaling model for *M*-log A observations of continental earthquakes, *Bull. Seismol. Soc. Am.*, *92*(5), 1841–1846, doi:10.1785/0120010148.

Heermance, R., Z. K. Shipton, and J. P. Evans (2003), Fault structure control on fault slip and ground motion during the 1999 rupture of the Chelungpu fault, Taiwan, *Bull. Seismol. Soc. Am.*, *93*, 1034–1050, doi:10.1785/0120010230.

Hirono, T., et al. (2008), Characterization of slip zone associated with the 1999 Taiwan Chi-Chi earthquake: X-ray CT image analyses and microstructural observations of the Taiwan Chelungpu fault, *Tectonophysics*, *449*, 63–84, doi:10.1016/j.tecto.2007.12.002.

Hirose, T., and T. Shimamoto (2005), Growth of molten zone as a mechanism of slip weakening of simulated faults in gabbro during frictional melting, *J. Geophys. Res.*, *110*, B05202, doi:10.1029/2004JB003207.

Ida, Y. (1972), Cohesive force across tip of a longitudinal-shear crack and Griffiths specific surface energy, *J. Geophys. Res.*, *77*(20), 3796, doi:10.1029/JB077i020p03796.

Ide, S. (2002), Estimation of radiated energy of finite-source earthquake models, *Bull. Seismol. Soc. Am.*, *92*(8), 2994–3005, doi:10.1785/0120020028.

Ide, S., and M. Takeo (1997), Determination of constitutive relations of fault slip based on seismic wave analysis, *J. Geophys. Res.*, *102*(B12), 27,379–27,391, doi:10.1029/97JB02675.

Jeffreys, H. (1942), On the mechanics of faulting, *Geol. Mag.*, *79*, 291–295, doi:10.1017/S0016756800076019.

Kanamori, H., and L. Rivera (2006), Energy partitioning during an earthquake, in *Earthquakes: Radiated Energy and the Physics of Faulting*, *Geophys. Monogr. Ser.*, vol. 170, edited by R. E. Abercrombie et al., pp. 193–198, AGU, Washington, D. C.

Kanamori, H., and G. S. Stewart (1978), Seismological aspects of Guatemala earthquake of February 4, 1976, *J. Geophys. Res.*, *83*(B7), 3427–3434, doi:10.1029/JB083iB07p03427.

Killick, A. M., and C. Roering (1998), An estimate of the physical conditions of pseudotachylite formation in the West Rand goldfield, Witwatersrand basin, South Africa, *Tectonophysics*, *284*(3–4), 247–259, doi:10.1016/S0040-1951(97)00181-9.

King, G., and J. Nabelek (1985), Role of fault bends in the initiation and termination of earthquake rupture, *Science*, *228*(4702), 984–987, doi:10.1126/science.228.4702.984.

Kirkpatrick, J. D., Z. K. Shipton, J. P. Evans, S. Micklethwaite, S. J. Lim, and P. McKillop (2008), Strike-slip fault terminations at seismogenic depths: The structure and kinematics of the Glacier Lakes fault, Sierra Nevada, United States, *J. Geophys. Res.*, *113*, B04304, doi:10.1029/2007JB005311.

Kirkpatrick, J. D., Z. K. Shipton, and C. Persano (2009), Pseudotachylytes: Rarely generated, rarely preserved, or rarely reported?, *Bull. Seismol. Soc. Am.*, *99*(1), 382–388, doi:10.1785/0120080114.

Lachenbruch, A. H. (1980), Frictional heating, fluid pressure, and the resistance to fault motion, *J. Geophys. Res.*, *85*(B11), 6097–6112, doi:10.1029/JB085iB11p06097.

Lin, A. M. (1996), Injection veins of crushing-originated pseudotachylyte and fault gouge formed during seismic faulting, *Eng. Geol. Amsterdam*, *43*(2–3), 213–224, doi:10.1016/0013-7952(96)00062-2.

Lu, K., E. E. Brodsky, and H. P. Kavehpour (2007), Shear-weakening of the transitional regime for granular flow, *J. Fluid Mech.*, *587*, 347–372, doi:10.1017/S0022112007007331.

Maddock, R. H. (1983), Melt origin of fault-generated pseudotachylytes demonstrated by textures, *Geology*, *11*(2), 105–108, doi:10.1130/0091-7613(1983)11<105:MOOFPD>2.0.CO;2.

Magloughlin, J. F., and J. G. Spray (1992), Frictional melting processes and products in geological-materials: Introduction and discussion, *Tectonophysics*, *204*(3–4), 197–206, doi:10.1016/0040-1951(92)90307-R.

Mai, P. M., and G. C. Beroza (2002), A spatial random field model to characterize complexity in earthquake slip, *J. Geophys. Res.*, *107*(B11), 2308, doi:10.1029/2001JB000588.

Marone, C., and B. Kilgore (1993), Scaling of the critical slip distance for seismic faulting with shear strain in fault zones, *Nature*, *362*(6421), 618–621, doi:10.1038/362618a0.

McKenzie, D., and J. N. Brune (1972), Melting on fault planes during large earthquakes, *Geophys. J. R. Astron. Soc.*, *29*(1), 65–78.

Melosh, H. J. (1996), Dynamical weakening of faults by acoustic fluidization, *Nature*, *379*(6566), 601–606, doi:10.1038/379601a0.

Mikumo, T., K. B. Olsen, E. Fukuyama, and Y. Yagi (2003), Stress-breakdown time and slip-weakening distance inferred from slip-velocity functions on earthquake faults, *Bull. Seismol. Soc. Am.*, *93*(1), 264–282, doi:10.1785/0120020082.

Miller, G. M., and D. S. Cowan (1998), Mesoscopic ductility in fault gouges, in *Fault-Related Rocks: A Photographic Atlas*, edited by A. W. Snoke et al., pp. 66–67, Princeton Univ. Press, Princeton, N. J.

Mizoguchi, K., T. Hirose, T. Shimamoto, and E. Fukuyama (2008), Internal structure and permeability of the Nojima fault, southwest Japan, *J. Struct. Geol.*, *30*, 513–524, doi:10.1016/j.jsg.2007.12.002.

Monzawa, N., and K. Otsuki (2003), Comminution and fluidization of granular fault materials: Implications for fault slip behavior, *Tectonophysics*, *367*(1–2), 127–143, doi:10.1016/S0040-1951(03)00133-1.

Noda, H., and T. Shimamoto (2005), Thermal pressurization and slip-weakening distance of a fault: An example of the Hanaore fault, southwest Japan, *Bull. Seismol. Soc. Am.*, *95*(4), 1224–1233, doi:10.1785/0120040089.

Olsen, M. P., C. H. Scholz, and A. Leger (1998), Healing and sealing of a simulated fault gouge under hydrothermal conditions: Implications for fault healing, *J. Geophys. Res.*, *103*(B4), 7421–7430, doi:10.1029/97JB03402.

Otsuki, K., N. Monzawa, and T. Nagase (2003), Fluidization and melting of fault gouge during seismic slip: Identification in the Nojima fault zone and implications for focal earthquake mechanisms, *J. Geophys. Res.*, *108*(B4), 2192, doi:10.1029/2001JB001711.

Otsuki, K., T. Uduki, N. Monzawa, and H. Tanaka (2005), Clayey injection veins and pseudotachylyte from two boreholes penetrating the Chelungpu fault, Taiwan: Their implications for the contrastive seismic slip behaviors during the 1999 Chi-Chi earthquake, *Isl. Arc*, *14*, 22–36, doi:10.1111/j.1440-1738.2004.00455.x.

Pachell, M. A., J. P. Evans, and W. L. Taylor (2003), Kilometer-scale kinking of crystalline rocks in a transpressive convergent setting, central Sierra Nevada, California, *Geol. Soc. Am. Bull.*, *115*(7), 817–831, doi:10.1130/0016-7606(2003)115<0817:KKOCRI>2.0.CO;2.

Peyrat, S., K. B. Olsen, and R. Madariaga (2004), Which dynamic rupture parameters can be estimated from strong ground motion and geodetic data?, *Pure Appl. Geophys.*, *161*(11–12), 2155–2169, doi:10.1007/s00024-004-2555-9.

Pittarello, L., G. Di Toro, A. Bizzarri, G. Pennacchioni, J. Hadizadeh, and M. Cocco (2008), Energy partitioning during seismic slip in pseudotachylyte-bearing faults (Gole Larghe fault, Adamello, Italy), *Earth Planet. Sci. Lett.*, *269*(1–2), 131–139, doi:10.1016/j.epsl.2008.01.052.

Rice, J. R. (2006), Heating and weakening of faults during earthquake slip, *J. Geophys. Res.*, *111*, B05311, doi:10.1029/2005JB004006.

Rice, J. R., and M. Cocco (2007), Seismic fault rheology and earthquake dynamics, in *Tectonic Faults: Agents of Change on a Dynamic Earth*, edited by M. R. Handy et al., pp. 99–137, MIT Press, Cambridge, Mass.

Rivera, L., and H. Kanamori (2002), Spatial heterogeneity of tectonic stress and friction in the crust, *Geophys. Res. Lett.*, *29*(6), 1088, doi:10.1029/2001GL013803.

Rowe, C. D., J. C. Moore, F. Meneghini, and A. W. McKeirnan (2005), Large-scale pseudotachylytes and fluidized cataclasites from an ancient subduction thrust fault, *Geology*, *33*(12), 937–940, doi:10.1130/G21856.1.

Scholz, C. H. (2002), *The Mechanics of Earthquakes and Faulting*, Cambridge Univ. Press, New York.

Schulz, S. E., and J. P. Evans (2000), Mesoscopic structure of the Punchbowl fault, southern California and the geologic and geophysical structure of active strike-slip faults, *J. Struct. Geol.*, *22*(7), 913–930, doi:10.1016/S0191-8141(00)00019-5.

Segall, P., E. H. McKee, S. J. Martel, and B. D. Turrin (1990), Late cretaceous age of fractures in the Sierra Nevada batholith, California, *Geology*, *18*(12), 1248–1251.

Sekiguchi, H., K. Irikura, and T. Iwata (2000), Fault geometry at the rupture termination of the 1995 Hyogo-ken Nanbu earthquake, *Bull. Seismol. Soc. Am.*, *90*(1), 117–133, doi:10.1785/0119990027.

Sibson, R. H. (1973), Interactions between temperature and pore-fluid pressure during earthquake faulting and a mechanism for partial or total stress relief, *Nature*, *243*(126), 66–68.

Sibson, R. H. (1975), Generation of pseudotachylyte by ancient seismic faulting, *Geophys. J. R. Astron. Soc.*, *43*(3), 775–794.

Sibson, R. H. (1977), Fault rocks and fault mechanisms, *J. Geol. Soc.*, *133*, 191–213, doi:10.1144/gsjgs.133.3.0191.

Sibson, R. H. (2003), Thickness of the seismic slip zone, *Bull. Seismol. Soc. Am.*, *93*(3), 1169–1178, doi:10.1785/0120020061.

Smith, S. A. F., C. Collettini, and R. E. Holdsworth (2008), Recognizing the seismic cycle along ancient faults: CO_2-induced fluidization of breccias in the footwall of a sealing low-angle normal fault, *J. Struct. Geol.*, *30*(8), 1034–1036, doi:10.1016/j.jsg.2008.04.010.

Wells, D. L., and K. J. Coppersmith (1994), New empirical relationships among magnitude, rupture length, rupture width, rupture area, and surface displacement, *Bull. Seismol. Soc. Am.*, *84*(4), 974–1002.

Wesnousky, S. G. (2006), Predicting the endpoints of earthquake ruptures, *Nature*, *444*(7117), 358–360, doi:10.1038/nature05275.

Wibberley, C. A. J., and T. Shimamoto (2005), Earthquake slip weakening and asperities explained by thermal pressurization, *Nature*, *436*(7051), 689–692, doi:10.1038/nature03901.

J. D. Kirkpatrick and Z. K. Shipton, Department of Geographical and Earth Sciences, University of Glasgow, Glasgow G12 8QQ, UK.